Monthly Notices
of the
ROYAL ASTRONOMICAL SOCIETY

MNRAS **467,** 2234–2240 (2017)
Advance Access publication 2017 January 25

doi:10.1093/mnras/stx210

Multifrequency study of a new hybrid morphology radio source

F. de Gasperin[1,2]★

[1]*Leiden Observatory, Leiden University, P.O.Box 9513, NL-2300 RA Leiden, the Netherlands*
[2]*Hamburg Observatory, University of Hamburg, Gojenbergsweg 112, D-21029 Hamburg, Germany*

Accepted 2017 January 23. Received 2017 January 20; in original form 2015 October 29

ABSTRACT

Hybrid morphology radio sources (HyMoRS) are a class of radio galaxies having the lobe morphology of a Fanaroff–Riley (FR) type I on one side of the active nucleus and of an FR type II on the other. The origin of the different morphologies between FR I and FR II sources has been widely discussed in the past 40 yr, and HyMoRS may be the best way to understand whether this dichotomy is related to the intrinsic nature of the source and/or to its environment. However, these sources are extremely rare ($\lesssim$1 per cent of radio galaxies), and only for a few of them, a detailed radio study that goes beyond the morphological classification has been conducted. In this paper, we report the discovery of one new HyMoRS; we present X-ray and multifrequency radio observations. We discuss the source morphological, spectral and polarization properties and confirm that HyMoRS are intrinsically bimodal with respect to these observational characteristics. We notice that HyMoRS classification based just on morphological properties of the source is hazardous.

Key words: galaxies: active – galaxies: individual: NVSS J232147+482956 – galaxies: individual: NVSS J232149+484951 – galaxies: nuclei – radio continuum: galaxies.

1 INTRODUCTION

Fanaroff & Riley (1974) divided radio galaxies into two categories based on their morphology. Fanaroff–Riley type I (FR I) galaxies have slower, more turbulent and less collimated jets. Conversely, FR II galaxies have powerful collimated jets (often only one is visible) that terminate into bright, compact 'hotspots'. In these regions, much of the bulk energy of the jet is converted into accelerating relativistic particles and amplifying magnetic fields through shocks produced by the beam against the intergalactic medium (Blandford & Rees 1974; Carilli et al. 1991). While the FR I class is made up of sources with different morphologies, the majority of them show jets that appear laminar in the innermost region inflating turbulent lobes after passing through a flare point. This characteristic can be well explained by the interaction with the ambient medium (Laing & Bridle 2014). The magnetic field orientation for FR I jets is often perpendicular to the jet, apart from the innermost region. Conversely, FR II jets have a magnetic field parallel to the jet orientation (Bridle 1984).

Another distinction between FR I and FR II was based on jet/lobe luminosity, with FR I having a lower luminosity ($<10^{25}$ W Hz^{-1} at 1.4 GHz) than FR II. The value of the radio luminosity transition depends on the properties of the host galaxies as it tends to increase with the host optical luminosity (Ledlow & Owen 1996), but this result has not been confirmed by subsequent analysis (Best 2009; Wing & Blanton 2010). This has been interpreted as a link between the morphological dichotomy of radio galaxies and the properties of either the nucleus (e.g. Ghisellini & Celotti 2001) or the environment (e.g. Bicknell 1995). FR I galaxies are found in richer clusters (Prestage & Peacock 1988) and this relation evolves in time, while at high-z, FR II galaxies are also found in cluster centres (Hill & Lilly 1991).

A peculiar sub-class of radio galaxies have a hybrid FR I/FR II morphology. Hybrid morphology radio sources (HyMoRS) were first defined by Gopal-Krishna & Wiita (2000) as a 'class of double radio sources in which the two lobes exhibit clearly different Fanaroff–Riley morphologies'. Gawronski et al. (2006) inspected 1700 sources from the FIRST survey, finding three certain and two possible HyMoRS, showing that these types of sources are rare ($\lesssim$1 per cent of radio galaxies belong to this category). Currently, around 10 HyMoRS are considered genuine, but only a small fraction of them have been studied in detail. Pirya et al. (2011) made a detailed multiwavelength radio study of two possible HyMoRS (J1211+743 and J1918+742). While, in other wavelengths, Miller & Brandt (2009) made *Chandra* observations of the two hybrids 3C 433 and 4C 65.15. They found that both sources have unabsorbed X-ray luminosity, radio luminosity and optical spectra of a typical FR II, while the FR I side is likely a consequence of jet–medium interaction. Finally, Ceglowski, Gawronski & Kunert-Bajraszewska (2013) examined the central 10 kpc of five known HyMoRS using VLBI observations. Their work underlines that genuine HyMoRS are not a consequence of the jet orientation, and that on 1–10-kpc scale their targets have weak jets, compatible with FR II-like

★ E-mail: fdg@strw.leidenuniv.nl

Table 1. Radio observations.

Telescope	Frequency (MHz)	Observation date	Total observing time (hr)	Bandwidth (MHz)	Maximum resolution (arcsec)	rms noise (μJy beam^{-1})	Figure
GMRT	323	2014 June 2	9	32	10.5 × 8.2	92	1 (top left-hand panel)
GMRT	607	2014 June 6	8	32	5.4 × 5.3	47	1 (top right-hand panel)
WSRT	1381	2014 January 2	8	160	17.3 × 13.3	32	1 (bottom left-hand panel)
VLA	1519	2015 April 2/5; 2016 January 30	10[a]	1000	4.8 × 4.3	10	1 (bottom right-hand panel)

Notes. [a]6 h in B configuration and 4 h in C configuration.

structures. The study of hybrid radio sources might be of fundamental importance to understand the origin of the FR dichotomy and assess whether the large-scale morphology of radio galaxies is linked to the central engine property, the environment or to a combination of the two.

Even though recent efforts have been undertaken to find hybrid sources, the known population of HyMoRS is still small, and, to our knowledge, no study has so far combined high-resolution, polarization and spectral index radio maps to characterize a candidate HyMoRS. In this paper, we report the discovery of a new HyMoRS: NVSS J232149+484951 (hereafter RG1). In Section 2, we present multifrequency observations of the source, and we analyse high-resolution and polarization radio maps. In Section 3, we present the newly discovered HyMoRS, and we make spectral index characterization in Section 3.1. In Section 4, we discuss another radio galaxy (NVSS J232147+482956, hereafter RG2) as an example of the difficulties in the HyMoRS classification when using only morphological data. Discussion and conclusions are in Section 5.

Throughout this paper, we adopt a fiducial Λ cold dark matter cosmology with $H_0 = 70\,\mathrm{km\,s^{-1}\,Mpc^{-1}}$, $\Omega_\mathrm{m} = 0.3$ and $\Omega_\Lambda = 0.7$. At the redshift of the target ($z \approx 0.16$), 1 arcsec = 2.8 kpc. All regressions are made with a bootstrap least-squares algorithm that takes into account errors on the dependant variables. Unless otherwise specified, errors are at 1σ. The spectral index is defined as $F_\nu \propto \nu^\alpha$, where F_ν is the flux density.

2 OBSERVATIONS AND DATA REDUCTION

2.1 Radio

We obtained GMRT data at 323 and 607 MHz, WSRT data at 1380 MHz and VLA data at 1–2 GHz (see Table 1). The observations are pointed towards the nearby galaxy cluster PSZ1 G108.18−11.53 ($z = 0.335$), but both radio galaxies described in this paper fall well within the primary beam full width at half-maximum (FWHM) of these observations. The data reduction procedures for the GMRT and WSRT observations are described in de Gasperin et al. (2015) and take advantage from the SPAM (Source Peeling and Atmospheric Modeling) package for ionospheric calibration to achieve high-fidelity, thermal noise limited images (Intema et al. 2009).

VLA data have been taken in the *L* band (1–2 GHz) in B and C configurations. The data were reduced using the CASA[1] package. The visibilities were Hanning smoothed, bandpass calibrated and flagged using the automatic tool AOFLAGGER (Offringa, van de Gronde & Roerdink 2012). We used 3C147 as the flux calibrator and 3C138 to calibrate the polarization angle. The flux scale has been set to Perley & Butler (2013), which above 1 GHz is in line with Scaife & Heald (2012) used for the low-frequency observations. Bandpass, scalar delays, cross-hand delays and polarization angle corrections were transferred to the target and phase calibrator. Then, the phase and rescaled amplitude from the phase calibrator were transferred to the target field. Finally, a single cycle of phase-only self-calibration was applied on the target field.

We note that all flux density errors for extended emission are computed as $S_\mathrm{err} = \sigma \cdot \sqrt{N_\mathrm{beam}}$, where σ is the local image rms and N_beam is the number of beams covering the source extension.

2.2 Optical

Although pointed-optical observations of the nearby clusters PSZ1 G108.18−11.53 are available, none of them cover the region of the hosting galaxy of RG1 or RG2. The redshift of both galaxies is currently unknown, but a photometric redshift should be included in the forthcoming release of PanSTARSS. To have a rough estimation of the redshift of RG1, we compared the *WISE* (W1- and W2-band) fluxes of RG1 with the redshift distribution of sources in the SAGE (Semi-Analytic Galaxy Evolution; Croton et al. 2016) models with comparable *WISE* fluxes and colours (see Fig. 2). The predicted redshift probability density function, $P(z)$, was generated by averaging the redshift distributions of photometrically similar sources in five model lightcones with different sightlines. The model photometry was generated using the FSPS (Flexible Stellar Population Synthesis) stellar population models (Conroy & Gunn 2009) and assuming a Chabrier initial mass function (Chabrier 2003). Additionally, dust attenuation is incorporated into the model photometry following the method outlined in Tonini et al. (2012). However, given the long wavelength of the filters being used, the effect of dust on the apparent magnitudes of model sources is likely very small. The most likely redshift is around $z = 0.16$, but this estimation must be taken just as a qualitative indication, and it will not be used to derive any important conclusion in the rest of this paper.

2.3 X-ray

A *Chandra* ACIS-I observation of 27 ks (obs. 801493, performed on 2014 September 23), pointed on the nearby cluster PSZ1 G108.18−11.53, has been reduced following the strategy described in van Weeren et al. (2016). The only significant emission that is associated with the candidate HyMoRS RG1 is co-located with the radio galaxy core (see Fig. 3). Given the number of photons detected, we were able to fit only a simple power law. Galactic N_H absorption was fixed at 1.25×10^{21} cm^{-2} (Kalberla et al. 2005). We obtained a slope of the electron distribution equal to 1.67 ± 0.21. The fit is shown in Fig. 4, and although the noise is large, it does not show evidence for strong internal absorption.

[1] https://casa.nrao.edu/

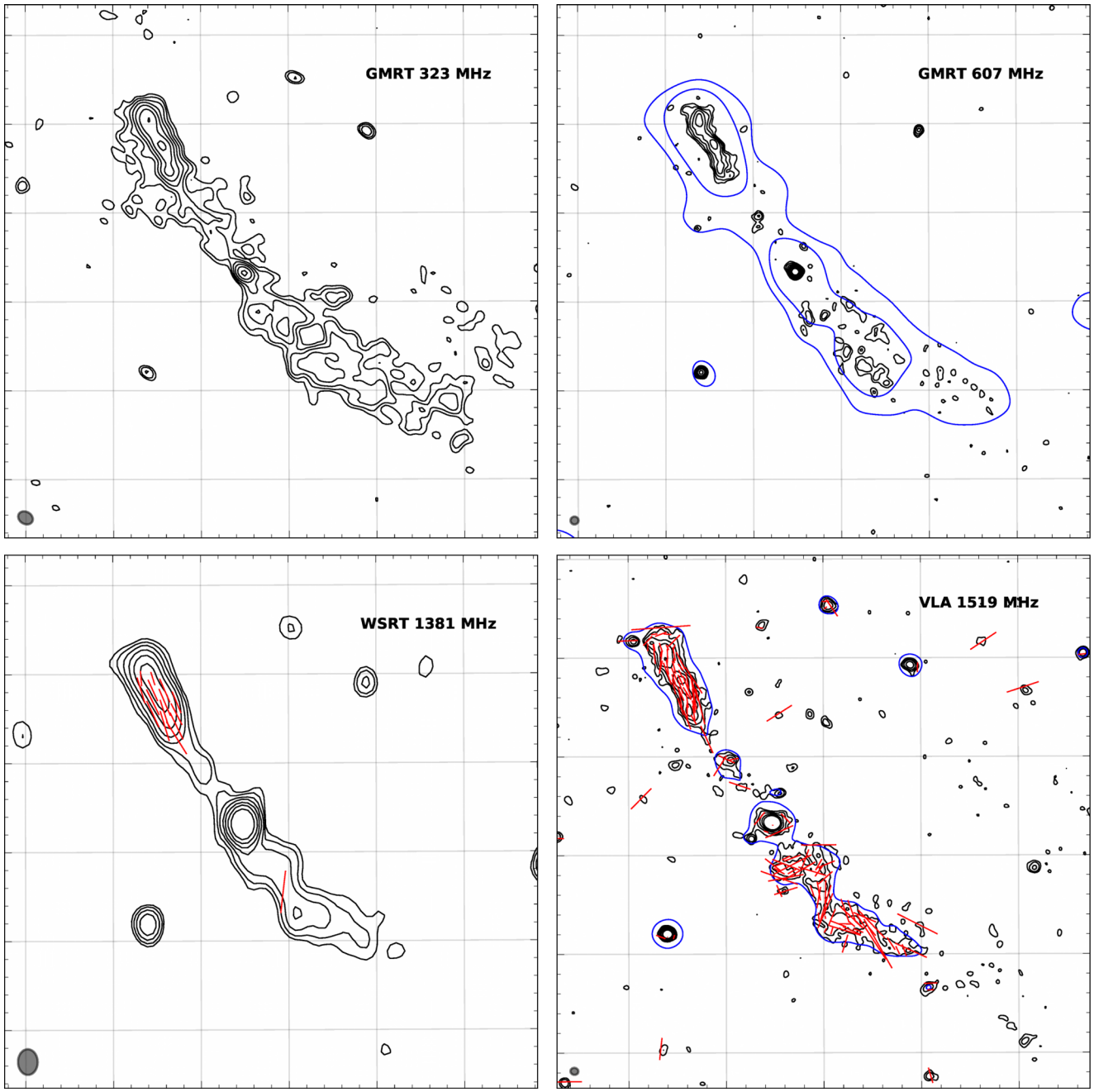

Figure 1. Black contours are from GMRT/WSRT/VLA data (323, 607, 1381 and 1519 MHz, as labelled in the images) at 3–30σ with sigma and beam size as described in Table 1. Blue contours are (3, 6)σ from a low-resolution image ($\sigma = 170$ μJy beam^{-1}, beam $= 18 \times 18$ arcsec^2 for GMRT 607 MHz and $\sigma = 15$ μJy beam^{-1}, beam $= 11 \times 10$ arcsec^2 for VLA 1519 MHz). Polarization vectors show the B mode (parallel to magnetic field orientation) with a length proportional to the fractional polarization, which, for the VLA image, is on average 18 per cent in the northern lobe and 35 per cent at the end of the southern lobe. Polarization angle has been corrected for Galactic rotation, which in this region of the sky is expected to be -14 rad m^{-2}(Oppermann et al. 2012).

3 A TRUE HyMoRS: NVSS J232149+484951 (RG1)

RG1 is likely not part of the cluster PSZ1 G108.18−11.53 but rather a foreground object. This conclusion is based on its distance from the cluster centre and angular size. The rough redshift estimation made in Section 2.2 ($z = 0.16$) also places the source in the foreground with respect to the cluster ($z = 0.335$). Assuming that redshift, the radio galaxy has a luminosity at 1.4 GHz of $(1.16 \pm 0.02) \times 10^{24}$ W Hz^{-1}. According to the historical FR I/FR II luminosity division (Owen & Ledlow 1994), the source would fall in the FR I regime; however, it is now known that both the morphological modes populate these luminosity ranges (Best 2009). The luminosity in the infrared (*WISE* at 12 μm, $\log(\nu L_\nu/\mathrm{erg\,s^{-1}}) = 42.7$), X-ray [*Chandra* 2–10 keV, $\log(L_{\mathrm{unabs}}/\mathrm{erg\,s^{-1}}) = 43.0$] and radio [178 MHz, $\log(\nu L_\nu/\mathrm{erg\,s^{-1}}) = 40.3$] points towards a classification as a low-excitation radio galaxy (LERG, Mingo et al. 2014).

The extension of RG1 is approximately 5 arcmin, which corresponds to a projected linear size of 840 kpc at $z = 0.16$. The nucleus of the source has a faint infrared *WISE* counterpart, an optical DSS counterpart (Fig. 5) and an X-ray *Chandra* counterpart (Fig. 3)

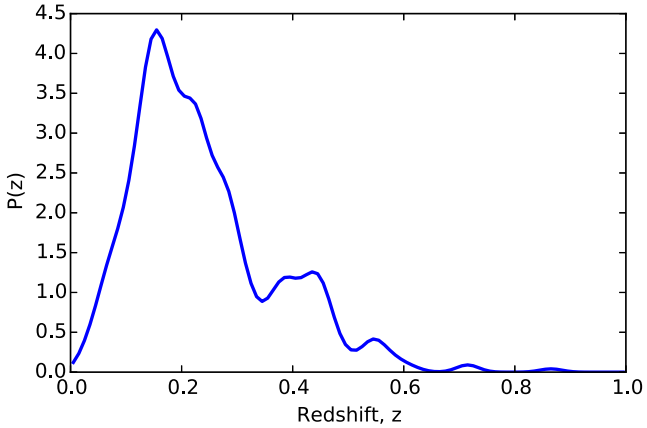

Figure 2. Normalized redshift probability density function of sources with W1 and W2 magnitudes within 2σ of RG1 for a set of semi-analytic models from SAGE (Croton et al. 2016). The peak of the distribution is at $z = 0.16$.

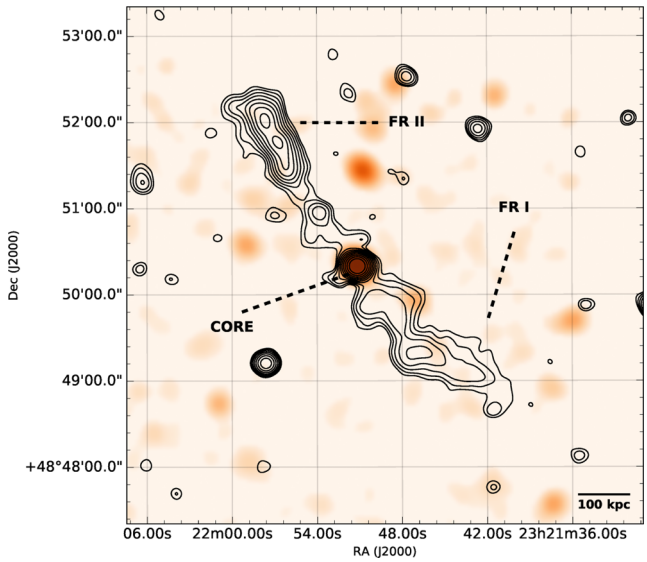

Figure 3. *Chandra* X-ray image of the field surrounding RG1. A few point sources are visible, one is co-located with the HyMoRS core, no X-ray excess is present in the location of the expected FR II hotspot. Radio contours are from a VLA image at 1519 MHz: (3–100)σ, logarithmically spaced, with $\sigma = 15$ μJy beam^{-1} (beam: 11×10 arcsec^2).

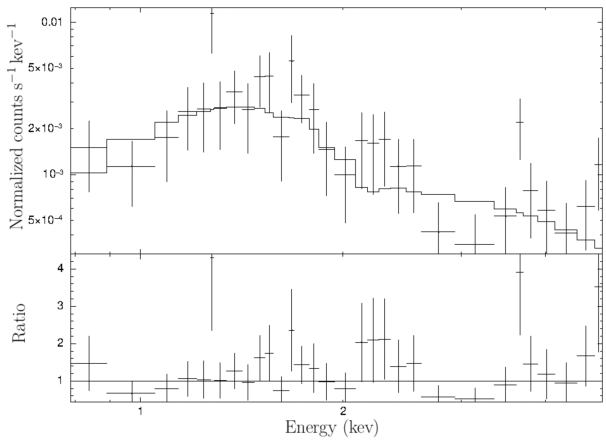

Figure 4. X-ray spectra of the point source co-located with the core of RG1.

at RA: $23^h21^m51^s.1$, Dec.: $48^\circ50'20''$. The active galactic nucleus is also identifiable in the spectral index map as a region with an inverted spectrum ($\alpha = +0.14 \pm 0.03$, Fig. 6).

The southern lobe has a clear FR I morphology. It is bent and does not have a clear termination point; instead, it fades into noise. The surface brightness is rather uniform along the lobe (see Fig. 7). The emission shows signs of polarization to an average level of 20 per cent. However, the magnetic field shows a quite disordered pattern, similar to the total intensity, which indicates a turbulent medium.

In contrast, the northern lobe has typical characteristics of FR II sources. The lobe brightness is enhanced towards its termination, and a discontinuity in the flux density, which increases by a factor of 3, is detected in the same region where the spectral index flattens (Fig. 7). In the location of enhanced brightness, the lobe emits 16 per cent polarized radiation. The magnetic field orientation is parallel to the jet direction, as seen in FR II sources (Bridle 1984). However, no prominent single hotspot is detected in that region. We report instead three surface brightness peaks aligned with the jet, which might indicate the presence of multiple hotspots (as seen in other radio sources like 3C 20, 3C 405 and 3C 351; Hardcastle & Looney 2008). No X-ray emission is detected in the location of the hotspot, which is not uncommon and has been reported for a number of bona fide FR II radio galaxies (see e.g. Hardcastle et al. 2004). RM synthesis can be a useful tool to study the inhomogeneous medium around HyMoRS cores. However, in this case, it does not show relevant features, and the measured Faraday depth in both lobes is compatible with being generated by our Galaxy (-14 rad m^{-2}, Oppermann et al. 2012).

3.1 Spectral analysis

Integrated flux density and spectral index values are listed in Table 2. More interesting is to study the spectral index profiles across the source extensions as they are distinct markers of FR I or FR II sources. In radio galaxies, the spectral energy distribution of the synchrotron emission is rather flat close to the location where electrons are accelerated. Synchrotron and inverse Compton losses deplete the more energetic electrons faster than the less energetic ones, steepening the spectrum with time. In the case of FR I sources, the jet is disrupted close to the central engine, and a steepening of the spectrum should be visible moving away from the core. In contrast, in FR II sources, the jet propagates relatively unperturbed until the 'hotspots', where it forms shocks that reaccelerate the electrons. These electrons then flow back towards the core. As a consequence, the radio spectra are expected to be flatter close to the hotspot and steeper close to the core, where the aged plasma accumulates.

To test these scenarios, we used the observations at 323 and 1519 MHz, where the most detailed radio images were obtained. The data sets were reimaged tapering the data so to obtain the same resolution (∼11 arcsec) in both maps. GMRT at 325 MHz and VLA at the *L* band in C configuration cover the same minimum *uv*-distance in wavelength, which means that the two interferometers are sensitive to the same maximum angular scale. This minimizes the bias due to the different *uv*-coverages, which is unavoidable when doing aperture synthesis of extended sources. Of the two images, we retained only pixels that were above 3σ in each map. We divided the source lobes into circular regions with a diameter twice the synthesized beam FWHM (see Fig. 6). For each region, we computed the integrated spectral index using a bootstrap least-squares

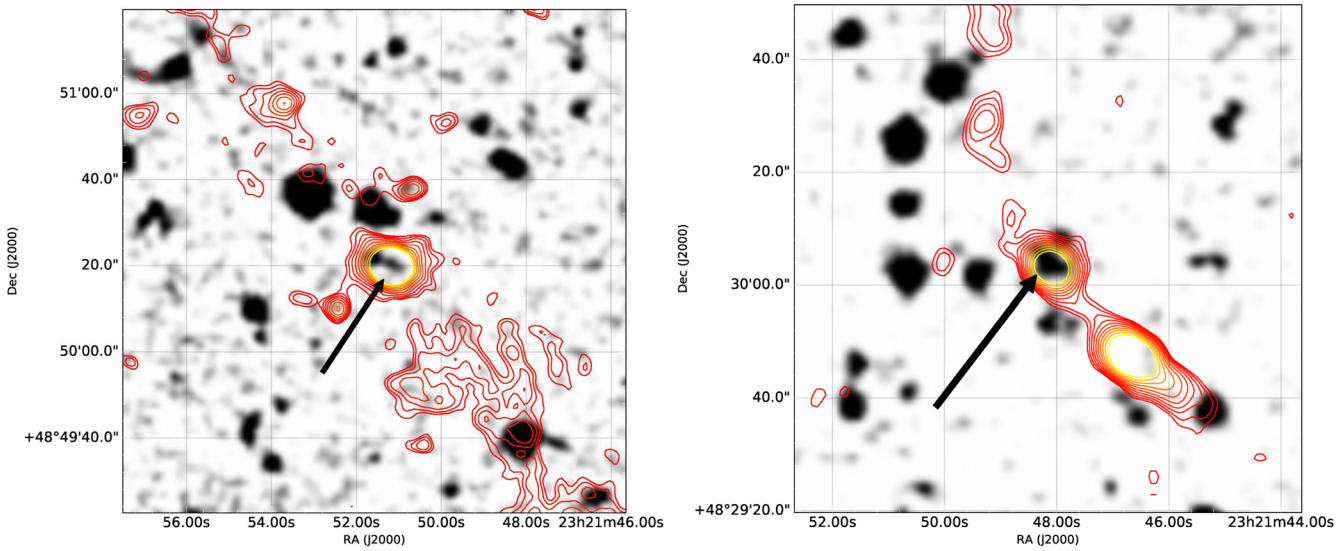

(a) RG1 (DSS) (b) RG2 (DSS)

Figure 5. DSS images (IR filter) of the cores of the HYMORS RG1 (left-hand panel) and the non-HYMORS RG2 (right-hand panel). Contours in the two panels are from the VLA images in Fig. 1 and Fig. 8, respectively. The optical counterparts are indicated by the arrow. The hosting galaxy might be in a merging state in both cases.

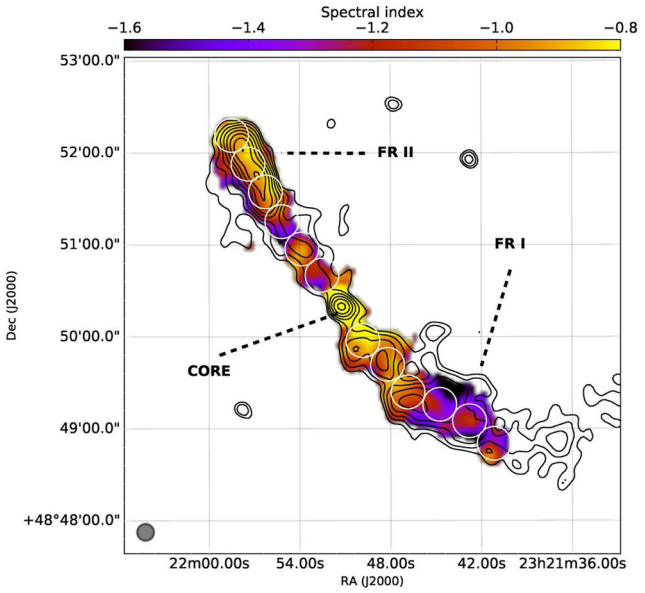

Figure 6. Spectral index maps obtained from the 1519- and 323-MHz maps. Overplotted the contours of the 323-MHz map at 3–50σ, logarithmically spaced, with $\sigma = 170$ μJy beam^{-1} and beam $= 18 \times 18$ arcsec^2 for both images. Dashed lines represent the regions used to extract the flux densities and spectral index values plotted in Fig. 7. The spectral index of the cores is rather flat, while gradients are seen in the lobes of RG1. The gradients are in line with the definition of FR I and FR II associated with the southern and the northern lobes, respectively. In contrast, RG2 does not show a clear gradient, but the spectral index allows us to identify the core position.

method to include flux density errors. The results of this analysis are shown in Fig. 7. RG1 shows opposite trends in the two lobes. The northern lobe has a steep spectral index ($\alpha = -1.2 \pm 0.1$) close to the core, which flattens in the outer region ($\alpha = -0.88 \pm 0.03$) due to particle reacceleration in the hotspot and back-flow of aged electrons towards the nucleus. The southern lobe has an opposite trend: The jet is disrupted close to the core and the electrons' spectra steepens from $\alpha = -0.86 \pm 0.06$ to -1.3 ± 0.1 due to synchrotron and inverse Compton losses as the distance from the core increases.

Morphology, polarization and spectral index characteristics all point to the classification of RG1 as a genuine HyMoRS.

4 CLASSIFICATION RISKS: NVSS J232147+482956 (RG2)

In this section, we present the analysis of another candidate HyMoRS that cannot be classified as such. This case exemplifies the danger of morphology-based classification of hybrid radio galaxies.

The core of RG2 is identifiable by a flat spectral index ($\alpha = -0.01 \pm 0.06$) and by a counterpart visible in the *WISE* and DSS images at RA: $23^h\,21^m\,48\overset{s}{.}1$, Dec: $48°30'04''$ (Fig. 5b). The northern lobe of the source has an FR I morphology, and it bends in two locations. Its spectral index is quite uniform along its extension ($\alpha \simeq -1$).

A compact emission close to the core is the brightest region of the source. It has a rather flat spectral index of $\alpha = -0.62 \pm 0.05$, and it is polarized to the level of ∼16 per cent. The polarization angle suggests a magnetic field oriented perpendicular to the jet direction as in the case of the initial part of the jet in FR I sources. We interpret this emission as beamed radiation from an incoming jet.

Low surface brightness emission is present 2 arcmin south-west of the core. This emission might be part of the source lobe. There is no apparent connection between this emission and the core-jet region, as has been seen in FR II lobes. However, the putative 'lobe' lacks a compact hotspot, and its spectral index is rather steep ($\alpha \lesssim -1$). We note the presence of a compact, flatter spectrum source (PS2 in Fig. 8, $\alpha = -0.77 \pm 0.06$) with no *WISE* nor DSS counterpart on the lobe's west side. A point source with a *WISE* counterpart is also present on the northern edge of this extended emission (PS3 in Fig. 8). An alternative interpretation could be that this extended emission is not part of the RG2 source, but it is a lobe related with the compact source PS3.

Table 2. Radio galaxies' flux densities.

	RA hh:mm:ss	Dec. dd:mm:ss	Flux 323 MHz[a] (mJy)	Flux 607 MHz[a] (mJy)	Flux 1380 MHz[a] (mJy)	Flux 1519 MHz[a] (mJy)	Integrated spectral index[b]
RG1 (HyMoRS)	23:21:51.1	48:50:20	78 ± 1	41 ± 1	15.0 ± 0.2	15.1 ± 0.3	-1.10 ± 0.01
RG2	23:21:48.1	48:30:04	41 ± 1	27 ± 1	12.1 ± 0.2	14.9 ± 0.3	-0.75 ± 0.02

Notes. [a]Flux density calculated within the 3σ contour of the 323 MHz map.
[b]Using all available frequencies.

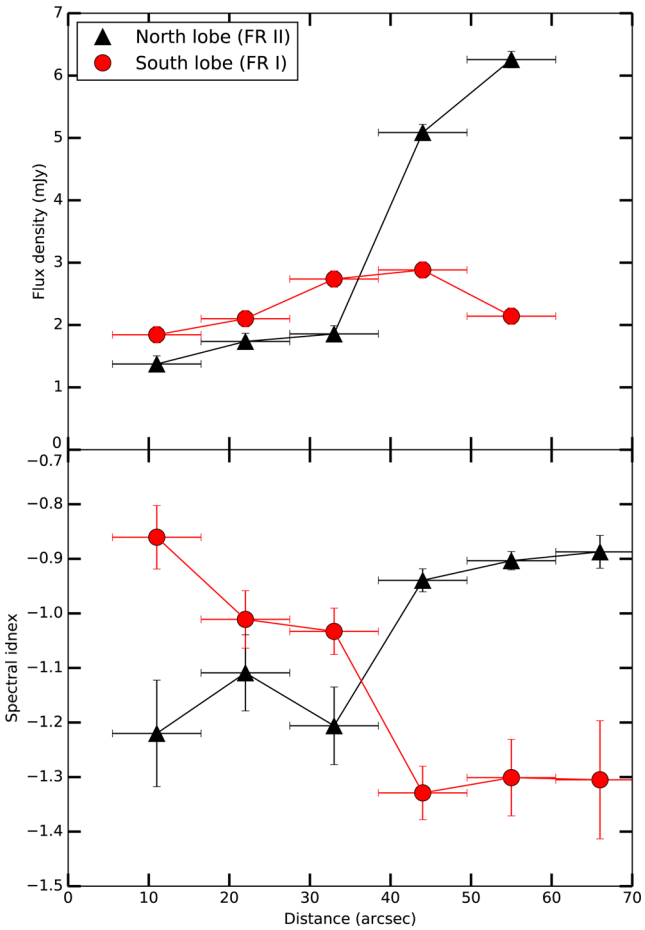

Figure 7. Top panel: integrated flux density at 323 MHz of the regions shown in Fig. 6. On the *x*-axis is the distance of the region from the source core; error bars are used to show the region extension. Bottom panel: integrated spectra index values of the regions shown in Fig. 6. The two lobes of RG1 show opposite trends as expected for HyMoRS. This is not the case for RG2, where both lobes are compatible with a constant spectral index along their extensions.

Although the source is difficult to interpret and probably strongly beamed, the data available to us do not suggest RG2 to be a hybrid radio galaxy. However, a low-resolution image (see Fig. 8) without spectral index or polarization information (as a radio survey image) could have led to the HyMoRS classification of RG2 based on its morphology.

5 DISCUSSION AND CONCLUSIONS

Some recent works support the idea that the FR I/FR II dichotomy might be related to environmental effects. In fact, in their central region, HyMoRS appear as FR II sources. This finding is supported by VLBI observations of the central 10 kpc (Ceglowski et al. 2013) and by measuring X-ray–radio scaling relations of the nuclear emission (Miller & Brandt 2009). In this scenario, one side of the source may decelerate and turn into an FR I type. A theoretical framework that can explain this behaviour was developed by Meliani, Keppens & Giacomazzo (2008), where the jet deceleration is caused by a density jump in the external medium. According to Perucho et al. (2012), the FR II type jet can also be disrupted by the growth of helical instability originated by the interaction with the surrounding media. It is interesting to notice that the magnetic field on the FR I side of RG1 seems indeed to trace an helical flow that might have disrupted the original FR II straight jet. Alternatively, the jets of FR II sources might be eroded by the entrainment due to the interactions with their surrounding lobes (Wang et al. 2011).

Other theories link the arising of an FR I or an FR II to the nucleus properties (Wold, Lacy & Armus 2007). However, X-ray and optical spectroscopic studies (Buttiglione et al. 2010; Best & Heckman 2012) support the division of radio sources based on line ratios (low-excitation galaxies or LEGs and high-excitation galaxies or HEGs) rather than their observed morphology, and link the discussion to the properties of the central engine: black hole spin or mode of accretion. In this classification, weak FR II galaxies (LEGs) fuelled via radiatively inefficient flows at low-accretion rates are grouped together with FR I galaxies (e.g. Best & Heckman 2012).

The picture that seems to arise is that all radio sources begin life as FR II sources, with collimated jets, but that some sources do not survive as such to large sizes, getting disrupted into FR I galaxies (Kaiser & Best 2007; Kunert-Bajraszewska et al. 2010). Therefore, the FR I/FR II nature of a radio galaxy must be related with both the central engine properties and accretion mode, which drives the jet power, as well as with the surrounding environment, which opposes the jet advancement. In this picture, HyMoRS are FR II sources with a jet power not much higher than that of an FR I. As a consequence, a variation in the environment around one of the two jets could cause its disruption and transformation in a turbulent FR I lobe.

In this work, we showed that HyMoRS have a complete bimodal nature under the point of view of morphology, polarization and spectral properties, showing no apparent difference between a 'standard' FR I (FR II) lobe and an HyMoRS FR I (FR II) lobe. We presented a multifrequency, polarimetric observation of two candidate HyMoRS. RG1 appears to be a rare example of an intrinsically true hybrid source as indicated by morphology, spectral index and polarization analysis. On the other hand, RG2 appears strongly beamed and does not show any hotspot on the putative FR II side and cannot be classified as an HyMoRS. Our work solidifies the importance to analyse multifrequency, high-resolution and polarization maps to accurately distinguish HyMoRS. More insight into the HyMoRS phenomenon will come from the analysis of larger samples that will be assembled soon, thanks to high-resolution, high-survey-speed telescopes such as LOFAR and SKA.

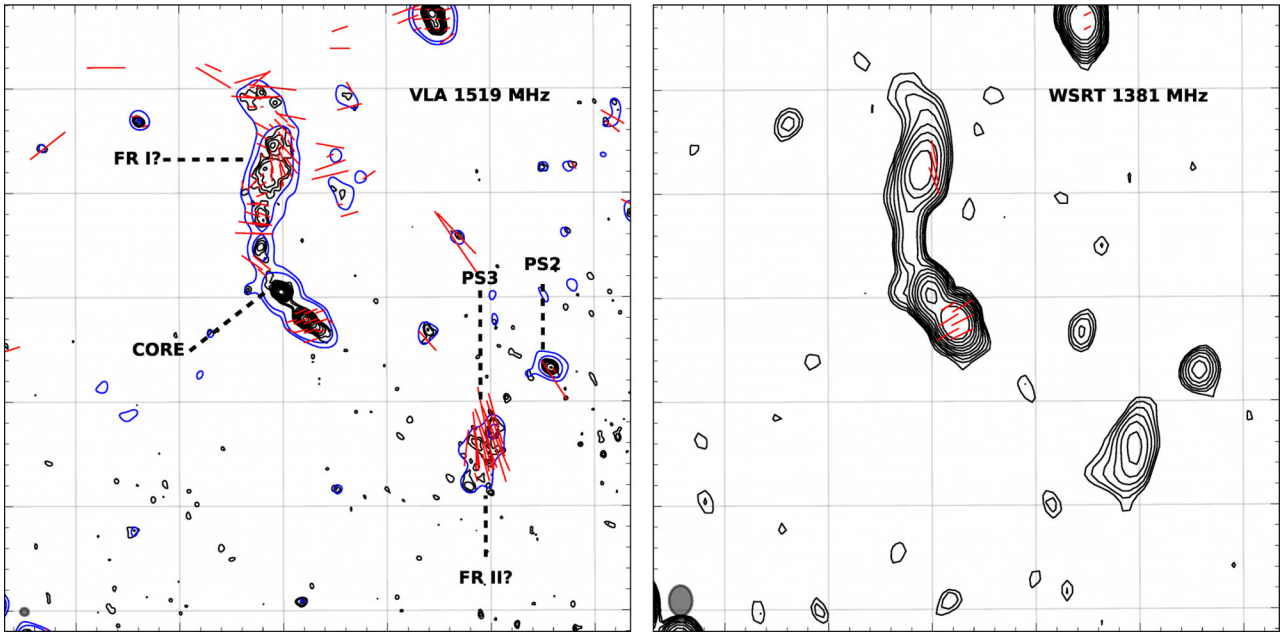

Figure 8. Radio images of RG2, a beamed FR I radio galaxy that cannot be classified as HyMoRS. Left-hand panel: black contours are from VLA data (1519 MHz) at 3–80σ, logarithmically spaced, with $\sigma = 20$ μJy beam^{-1}, beam $= 4.8 \times 4.3$ arcsec^2. Blue contours are (3, 6)σ from a low-resolution image ($\sigma = 35$ μJy beam^{-1}, beam $= 11 \times 11$ arcsec^2). Right-hand panel: contours from WSRT data (1381 MHz) at 3–50σ, logarithmically spaced, with $\sigma = 37$ μJy beam^{-1}, beam $= 17.3 \times 13.3$ arcsec^2. In both images, vectors trace the B modes of polarized emission.

ACKNOWLEDGEMENTS

The author would like to thank Marcus Brüggen, Philip Best, Reinout van Weeren and Kenneth Duncan for the discussions and suggestions.

We would like to thank the staff of the GMRT that made these observations possible. GMRT is run by the National Centre for Radio Astrophysics of the Tata Institute of Fundamental Research.

The National Radio Astronomy Observatory is a facility of the National Science Foundation operated under cooperative agreement by Associated Universities, Inc.

This work is part of the VENI research programme with project number 1808, which is financed by the Netherlands Organisation for Scientific Research (NWO).

REFERENCES

Best P. N., 2009, Astron. Nachr., 330, 184
Best P. N., Heckman T. M., 2012, MNRAS, 421, 1569
Bicknell G. V., 1995, ApJS, 101, 29
Blandford R. D., Rees M. J., 1974, MNRAS, 169, 395
Bridle A. H., 1984, AJ, 89, 979
Buttiglione S., Capetti A., Celotti A., Axon D. J., Chiaberge M., Macchetto F. D., Sparks W. B., 2010, A&A, 509, A6
Carilli C. L., Perley R. A., Dreher J. W., Leahy J. P., 1991, ApJ, 383, 554
Ceglowski M., Gawronski M., Kunert-Bajraszewska M., 2013, A&A, 557, A75
Chabrier G., 2003, Publ. Astron. Soc. Pac., 115, 763
Conroy C., Gunn J. E., 2009, ApJ, 712, 833
Croton D. J. et al., 2016, ApJS, 222, 22
de Gasperin F., Intema H. T., van Weeren R. J., Dawson W. A., Golovich N., Wittman D., Bonafede A., Brüggen M., 2015, MNRAS, 453, 3483
Fanaroff B. L., Riley J. M., 1974, MNRAS, 167, 31
Gawronski M. P., Marecki A., Kunert-Bajraszewska M., Kus A. J., 2006, A&A, 447, 63
Ghisellini G., Celotti A., 2001, A&A, 379, L1
Gopal-Krishna, Wiita P. J., 2000, A&A, 363, 507
Hardcastle M. J., Looney L. W., 2008, MNRAS, 388, 176
Hardcastle M. J., Harris D. E., Worrall D. M., Birkinshaw M., 2004, ApJ, 612, 729
Hill G. J., Lilly S. J., 1991, ApJ, 367, 1
Intema H. T., van der Tol S., Cotton W. D., Cohen A. S., van Bemmel I. M., Röttgering H. J. A., 2009, A&A, 501, 1185
Kaiser C. R., Best P. N., 2007, MNRAS, 381, 1548
Pöppel, W. G. L.Kalberla, Burton W. B., Hartmann D., Arnal E. M., Bajaja E., Morras R., P. M. W.2005, A&A, 440, 775
Kunert-Bajraszewska M., Gawroński M. P., Labiano A., Siemiginowska A., 2010, MNRAS, 408, 2261
Laing R. A., Bridle A. H., 2014, MNRAS, 437, 3405
Ledlow M. J., Owen F. N., 1996, AJ, 112, 1
Meliani Z., Keppens R., Giacomazzo B., 2008, A&A, 337, 321
Miller B. P., Brandt W. N., 2009, ApJ, 695, 755
Mingo B., Hardcastle M. J., Croston J. H., Dicken D., Evans D. A., Morganti R., Tadhunter C., 2014, MNRAS, 440, 269
Offringa A. R., van de Gronde J. J., Roerdink J. B. T. M., 2012, A&A, 539, A95
Oppermann N. et al., 2012, A&A, 542, A93
Owen F. N., Ledlow M. J., in Geoffrey B. V., Michael D. A., Peter Q. J., eds, 1994, ASP Conf. Ser. Vol. 54, The First Stromlo Symposium: The Physics of Active Galaxies. Astron. Soc. Pac., San Francisco
Perley R. A., Butler B. J., 2013, ApJS, 204, 19
Perucho M., Martí-Vidal I., Lobanov A. P., Hardee P. E., 2012, A&A, 545, A65
Pirya A., Nandi S., Saikia D. J., Singh M., 2011, Bull. Astron. Soc. India, 39, 547
Prestage R. M., Peacock J. A., 1988, MNRAS, 230, 131
Scaife A. M. M., Heald G. H., 2012, MNRAS, 423, 30
Tonini C., Bernyk M., Croton D., Maraston C., Thomas D., 2012, ApJ, 759, 43
van Weeren R. J. et al., 2016, ApJ, 818, 204
Wang Y., Knigge C., Croston J. H., Pavlovski G., 2011, MNRAS, 418, 1138
Wing J. D., Blanton E. L., 2010, AJ, 141, 88
Wold M., Lacy M., Armus L., 2007, A&A, 470, 531

This paper has been typeset from a TEX/LATEX file prepared by the author.